Cellular and Molecular Life Sciences (2023) 80:152
https://doi.org/10.1007/s00018-023-04800-0

ORIGINAL ARTICLE

BBOF1 is required for sperm motility and male fertility by stabilizing the flagellar axoneme in mice

Huiwen Cao[1] · Haomang Xu[1] · Yiqing Zhou[1] · Wei Xu[1] · Qinglin Lu[2] · Lingying Jiang[3] · Yan Rong[3] · Qianting Zhang[2,4] · Chao Yu[1,3]

Received: 30 January 2023 / Revised: 3 May 2023 / Accepted: 4 May 2023 / Published online: 17 May 2023

Abstract

The sperm flagellum is a specialized type of motile cilium composed of a typical "9 + 2" axonemal structure with peri-axonemal structures, such as outer dense fibers (ODFs). This flagellar arrangement is crucial for sperm movement and fertilization. However, the association of axonemal integrity with ODFs remains poorly understood. Here, we demonstrate that mouse BBOF1 could interact with both MNS1, an axonemal component, and ODF2, an ODF protein, and is required for sperm flagellar axoneme maintenance and male fertility. BBOF1 is expressed exclusively in male germ cells from the pachytene stage onwards and is detected in sperm axoneme fraction. Spermatozoa derived from *Bbof1*-knockout mice exhibit a normal morphology, however, reduced motility due to the absence of certain microtubule doublets, resulting in the failure to fertilize mature oocytes. Furthermore, BBOF1 is found to interact with ODF2 and MNS1 and is also required for their stability. Our findings in mice suggest that *Bbof1* could also be essential for human sperm motility and male fertility, thus is a novel potential candidate gene for asthenozoospermia diagnosis.

Keywords CASA · Fertilization · Microtubule doublets · Infertility · Asthenozoospermia

Introduction

In most species, the sperm flagellum or tail of spermatozoa is a crucial structure for the oscillatory movement of spermatozoa along the female reproductive tract to reach and fertilize mature oocytes [1, 2]. Defects in the sperm flagellum are direct causes of male infertility, manifested by varying degrees of oligoasthenoteratozoospermia (OAT), i.e., decreased sperm number, reduced motility, abnormal morphology, or a combination of them [3]. According to World Health Organization (WHO) recommendations, asthenozoospermia is characterized by < 42% motile spermatozoa or < 30% progressive spermatozoa, without significant changes in sperm count and morphology [4]. However, the genetic factors underlying asthenozoospermia remain poorly understood.

The axoneme is the central component of the sperm flagellum and spans throughout the length of the flagellum. Similar to other types of motile cilia, the axoneme of the sperm flagellum is composed of a typical "9 + 2" arrangement: a pair of central microtubule singlets surrounded by nine peripheral microtubule doublets (MTDs) with radial spokes, inner dynein arms (IDAs), outer dynein arms

Huiwen Cao, Haomang Xu, Yiqing Zhou and Wei Xu authors contributed equally.

✉ Qianting Zhang
qiantingzhang@zju.edu.cn

✉ Chao Yu
chao_yu@zju.edu.cn

1 College of Life Sciences, Zhejiang University, 866 Yuhangtang Road, Hangzhou 310058, China

2 Zhejiang University-University of Edinburgh Institute (ZJU-UoE Institute), Zhejiang University School of Medicine, Zhejiang University, 718 East Haizhou Road, Haining 314400, China

3 Key Laboratory of Reproductive Dysfunction Management of Zhejiang Province, Assisted Reproduction Unit, Department of Obstetrics and Gynecology, School of Medicine, Sir Run Run Shaw Hospital, Zhejiang University, 866 Yuhangtang Road, Hangzhou 310058, China

4 The Second Affiliated Hospital, Zhejiang University School of Medicine, Zhejiang University, Hangzhou, China

(ODAs), and other accessory structures connecting the microtubules [5]. Genetic mutations of more than 40 axonemal proteins have been reported to be associated with fertility, including proteins localized to IDA (DNAH1/2/6) [6–8], ODA (DNAH5/8/9/17, DNAI1/2, CFAP70) [9–15], central pair apparatus (SPEF2, CFAP58/65, SPAG6) [16–19], radial spoke (CFAP91/251, RSPH1/3/4A/9) [20–24] and centriole (CEP135, DZIP1) [25, 26], as well as proteins involved in MTD organization (CFAP43/44/47, CCDC39/40, GAS8) [27–31], assembly of dynein arms (DNAAF1-6, LRRC6, TTC12) [32–34], and intra-flagellar transport (TTC21A, TTC29, CFAP69) [35–37], etc. Mutations in these genes can lead to a disrupted axonemal structure and, therefore, severe malformation in sperm flagella, resulting in multiple morphological abnormalities of the flagella (MMAF) or primary ciliary dyskinesia (PCD), depending on whether the defects are seen in the flagella only or in both the flagella and motile cilia [32]. Mixed phenotypes of coiled, bent, irregular, short, or absent flagella, poor motility, decreased sperm counts, or OAT, are frequently observed in human patients or mice with mutations in these axonemal genes. Only a few genes have been reported to be pathogenic genes that underlie isolated asthenozoospermia [38, 39].

The mammalian sperm flagellum can be compartmentalized into three parts based on its internal ultrastructure [40, 41]. The mid-piece is closest to the sperm head and consists of an axoneme, outer dense fibers (ODFs), and a mitochondrial sheath, which provides energy to support flagellar movement. The principal piece is the longest region of the sperm flagellum and includes an axonemal structure surrounded by seven ODFs and two fibrous sheaths, whereas the end piece contains only the axoneme. ODFs are flagella-specific cytoskeletal structures that maintain the elasticity of the sperm to avoid shear force [40–43]. At least 14 proteins have been detected in mammalian ODFs, including ODF1–4 and other ODF-related proteins [44]. Several lines of evidence have shown that ODFs are required for the maintenance of axonemal integrity. Mice lacking ODF2 have been found to exhibit a disrupted axonemal structure and thus phenotypes of asthenozoospermia [43]. Reduced ODF protein levels have been detected in spermatozoa collected from patients with asthenozoospermia. On the other hand, in spermatozoa showing the lack of MTDs, such as those with mutations in *Qrich2* and *Dnah17*, the corresponding ODFs are often missing, suggesting that the integrity of the axoneme and ODFs are strongly interconnected [38, 45]. However, the underlying mechanisms remain unknown.

Basal body orientation factor 1 (BBOF1), also known as CCDC176, contains two coiled-coil domains and is evolutionarily conserved in vertebrates. Recently, *Xenopus* bbof1 has been characterized as a cilia-associated factor that is induced by the transcription factor foxj1 to mediate the alignment and orientation of cilia in epidermal multi-ciliated cells [46]. However, little is known about its function in mammals. In this study, we found that BBOF1 is required for sperm flagellar axoneme maintenance and male fertility in mice. BBOF1 expression is elevated during meiosis, and it is accumulated in round spermatids. BBOF1 deletion has compromised effects on growth, survival, and spermatogenesis, however leads to asthenozoospermia due to an incomplete axonemal ultrastructure and reduced motility. Moreover, BBOF1 could interact with both the axonemal component meiosis-specific nuclear structural 1 (MNS1) and the ODF protein ODF2. Taken together, our results suggested that BBOF1 plays an essential role in sperm motility and male fertility in mice by stabilizing the axonemal structure and that it is a structural component involved in coupling ODFs and the axoneme to facilitate axonemal stability.

Results

Testis-expressed BBOF1 is required for male fertility

We first assessed the expression pattern of BBOF1 in mice. According to the semi-quantitative RT-PCR results for cDNA samples derived from multiple mouse tissues, *Bbof1* was exclusively expressed in mouse testes (Fig. 1A). The expression of *Bbof1* in testes was first detected at PD16 (postnatal day 16), the time point when the first wave of spermatocytes enter the pachytene stage, and was increased with testis development from PD18 to PD69 (Fig. 1B). Specifically, we sorted spermatocytes and spermatids at different stages and found that the level of *Bbof1* mRNA was markedly increased in pachytene/diplotene spermatocytes and round spermatids (Fig. 1C; Supplementary Fig. 1A).

To investigate the physiological functions of BBOF1 in mammals, we generated a *Bbof1*-knockout mouse model using the CRISPR/Cas9 system. An sgRNA was designed to target exon 6 (E6) of *Bbof1* and was microinjected into wild-type (WT) mouse zygotes together with Cas9 protein (Fig. 1D). Through PCR amplification and sequencing, we identified a founder mouse with an overall 25 bp deletion within E6, which introduces a premature stop codon and produces a putative mutant protein with 212 amino acids (aa) in length (Fig. 1D). This allele (regarded as the knockout allele or null allele) was successfully transmitted to the next generation by backcrossing the founder mouse with WT mice. $Bbof1^{-/-}$ mice were obtained by interbreeding between heterozygous ($Bbof1^{+/-}$) males and females (Fig. 1E). The ablation of BBOF1 protein was confirmed by Western blotting of the testis lysates of $Bbof1^{-/-}$ mice (Fig. 1F). The percentage of $Bbof1^{-/-}$ progeny mice was in accordance with the Mendelian ratio (25.6%, $n = 215$), and no apparent defects in their viability, body weight, and external morphology had been observed (Supplementary Fig. 1B–C).

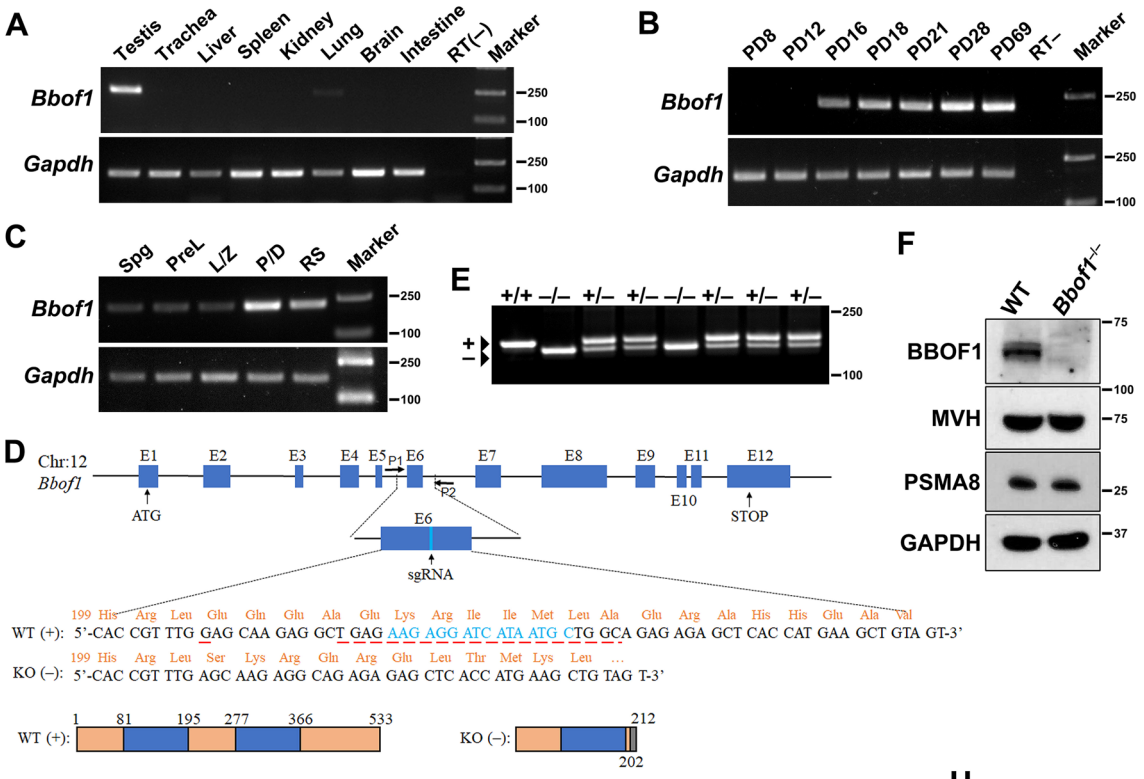

G

Genotype	Pups/Plug	Pups/litter	Litter/plug (%)	Plugs	Litters
♂+/– X ♀+/–	7.25 (±0.27)	7.25 (±0.27)	100	76	76
♂+/– X ♀–/–	7.24 (±0.53)	7.24 (±0.53)	100	17	17
♂–/– X ♀+/–	0.13 (±0.07)	1.25 (±0.35)	10.5	38	4

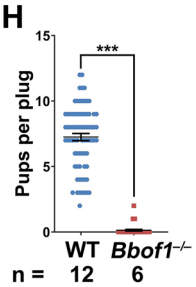

Fig. 1 BBOF1 is specifically expressed in mouse testes and is required for male fertility. **A–C**, Semi-quantitative RT-PCR showing the *Bbof1* mRNA level in samples derived from multiple tissues (**A**), testes at different ages (**B**), and male germ cells at different developmental stages (**C**). *Gapdh* was used as the loading control. *PD* postnatal day, *Spg* spermatogonia, *PreL* preleptotene, *L/Z* leptonema-zygonema, *P/D* pachynema-diplonema, *RS* round spermatids. **D** Schematic diagram illustrating the CRISPR/Cas9 strategy designed to generate the *Bbof1*-knockout allele. In comparison with the WT allele, the *Bbof1*-knockout allele has an overall 25 bp deletion within exon 6 (underlined in red) and encodes a putative 212-aa mutant protein due to the frameshift mutation (bottom). The sgRNA sequence (in brilliant blue) and genotyping primers (P1, P2) are indicated. **E** Representative genotyping image showing the different genotypes (*Bbof1*$^{+/+}$, *Bbof1*$^{+/–}$, and *Bbof1*$^{–/–}$). **F** Western blotting of the testes from WT and *Bbof1*$^{–/–}$ males at PD42. GAPDH was used as the loading control. **G–H** Fertility test of *Bbof1*$^{–/–}$ males and females. Pups per plug and pups per litter are presented as the mean (±S.E.M.) in Panel (**G**). Error bars in scatter plot (**H**) indicate the S.E.M. ***, $P<0.001$ (two-tailed Student's *t*-test). *n* indicates the number of males analyzed

We performed fertility tests on BBOF1-deficient males and females. According to the statistical analysis of progeny numbers in different mating groups, BBOF1 deletion severely impaired male fertility while did not affect female fertility (Fig. 1G–H). Adult *Bbof1*$^{–/–}$ males were able to mate with *Bbof1*$^{+/–}$ and WT females, as indicated by the presence of vaginal plugs; however, successful pregnancy was not guaranteed (4 litters from 38 plugs). Therefore, *Bbof1*$^{–/–}$ males exhibited a phenotype of subfertility, as demonstrated by the fertility test (0.13 pups per plug and 1.25 pups per litter, Fig. 1G–H).

BBOF1 is dispensable for spermatogenesis

Next, we investigated the effect of BBOF1 deletion on male fertility. Initially, we analyzed the testes and epididymides of adult WT and knockout males. Unexpectedly, the size and weight of the testes were not influenced by BBOF1

deletion (Fig. 2A–B). Hematoxylin and eosin staining of paraffin-embedded WT and *Bbof1*$^{-/-}$ testis tissue sections showed no apparent defects. All stages of spermatogenesis, spermatogonia, spermatocytes, round spermatids, and elongated spermatids were evident in the *Bbof1*$^{-/-}$ testis tissue sections (Supplementary Fig. 2A). Wilms' tumor 1 (WT1) is a marker of Sertoli cells and is required for the development of testicular cords during embryogenesis, and mouse Vasa homolog (MVH) is a marker of germ cells [47]. Immunofluorescence staining of WT1 and MVH showed no obvious

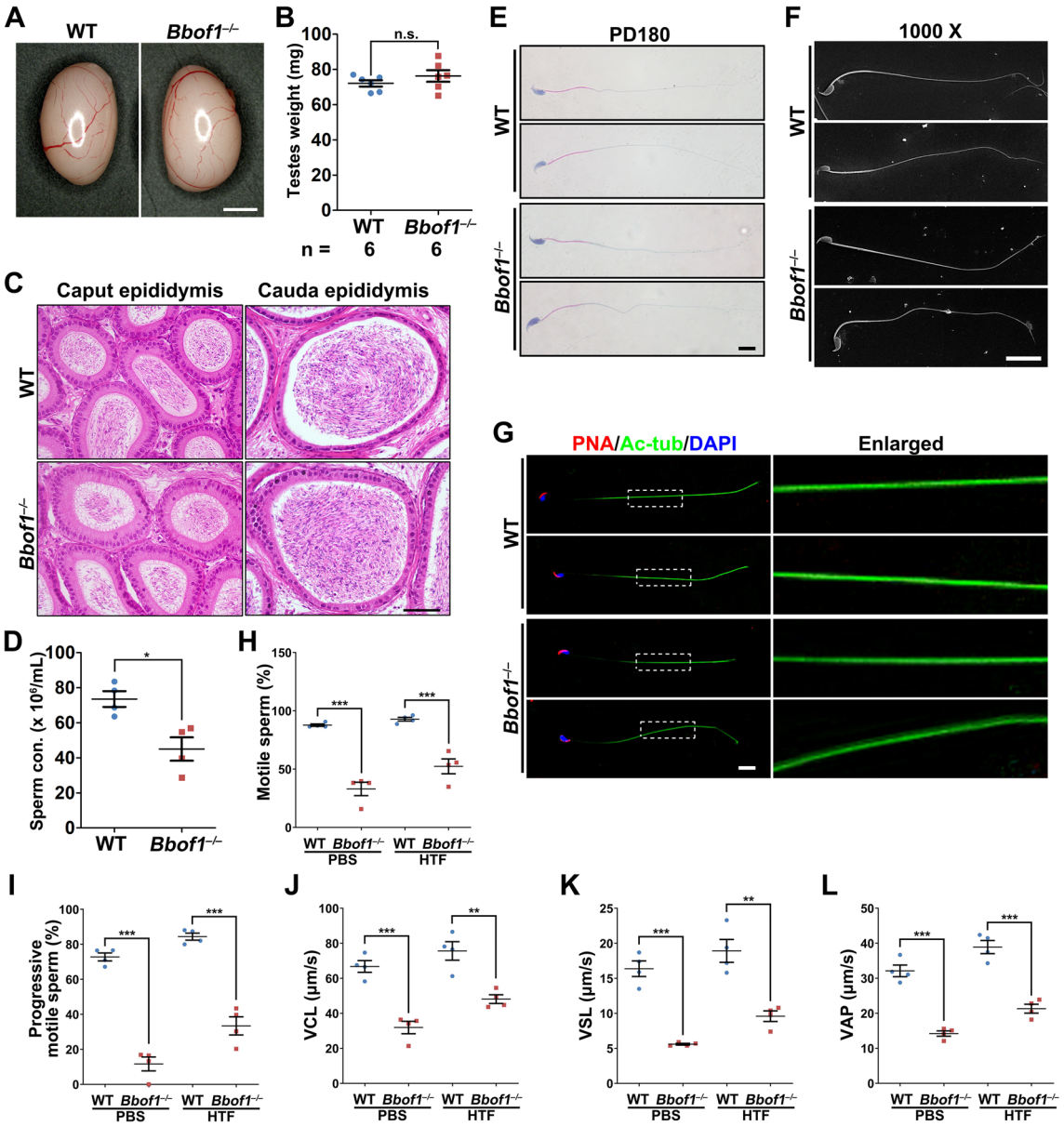

Fig. 2 BBOF1 deletion leads to reduced sperm motility. **A** Representative images of testes from WT and *Bbof1*$^{-/-}$ males at PD42. Scale bar, 1 mm. **B** Weights of WT and *Bbof1*$^{-/-}$ testes from PD42 males. The number of testes analyzed (*n*) is indicated. Error bars indicate the S.E.M. n.s., not significant (two-tailed Student's *t*-test). **C** H&E staining of epididymides sections derived from WT and *Bbof1*$^{-/-}$ males. Scale bars, 50 μm. **D** Quantification of the sperm concentration ($\times 10^6$/mL) in the semen of adult WT and *Bbof1*$^{-/-}$ males. Error bars indicate the S.E.M. *, $P < 0.05$ (two-tailed Student's *t*-test). **E** Papanicolaou staining showing the morphology of WT and *Bbof1*$^{-/-}$ spermatozoa. Scale bar, 10 μm. **F** Scanning electron microscopy (SEM) images showing the morphology of WT and *Bbof1*$^{-/-}$ spermatozoa. Scale bar, 20 μm. **G** Immunofluorescence staining of PNA (red) and acetylated α-tubulin (Ac-tub, green) with DAPI in spermatozoa. Scale bar, 10 μm. **H–I** Relative percentages of spermatozoa with motility and progressive motility from WT and *Bbof1*$^{-/-}$ males after incubation in PBS or HTF medium for 60 min. Error bars indicate the S.E.M. ***$P < 0.001$ (two-tailed Student's *t*-test). **J–L** Motility parameters for spermatozoa in (**D**) examined by CASA. *VCL* curvilinear velocity, *VSL* straight-line velocity, *VAP* average path velocity. Error bars indicate the S.E.M. **$P < 0.01$; ***$P < 0.001$ (two-tailed Student's *t*-test)

difference in the number of Sertoli cells or germ cells in *Bbof1*$^{-/-}$ testes (Supplementary Fig. 2B–C). PSMA8 has been identified as a subunit of the testis-specific 20S core proteasome, which accumulates in spermatocytes from the pachytene stage [48]. Similarly, γH2AX is a marker of the generation and repair of DNA double-strand breaks. PSMA8 signals and γH2AX signals indicated normal meiotic prophase I progression in BBOF1-deleted spermatocytes (Supplementary Fig. 2D–E).

Bbof1$^{-/-}$ males could produce spermatozoa with a normal morphology as their epididymides sections were full of mature spermatozoa (Fig. 2C). Peanut agglutinin (PNA) staining is often used to assess the Golgi-to-acrosome transition during spermiogenesis. PNA signals were not considerably different between WT and *Bbof1*$^{-/-}$ testes (Supplementary Fig. 2F). To determine the effects of BBOF1 deletion on both the quantity and quality of spermatozoa, they were collected from the cauda epididymides for examination in vitro. An approximate 30% decrease in sperm count and a slight decrease in the ratio of normal spermatozoa (93.35% in WT and 88.14% in *Bbof1*$^{-/-}$; P value = 0.025) were observed in *Bbof1*$^{-/-}$ males (Fig. 2D; Supplementary Fig. 3A). The morphology of spermatozoa and the incidence of abnormal spermatozoa were not dramatically affected by BBOF1 deletion (Fig. 2E–G; Supplementary Fig. 3A). Taken together, these results suggested that BBOF1 may be dispensable for spermatogenesis and the gross morphology of spermatozoa.

BBOF1 deletion leads to reduced sperm motility

However, the percentages of motile spermatozoa and progressive motile spermatozoa were significantly decreased in *Bbof1*$^{-/-}$ mice under both non-capacitation condition (PBS) and capacitation condition (HTF), which are common characteristics of asthenozoospermia (Fig. 2H–I; Supplementary Movie 1 and 2). Computer-assisted sperm analysis (CASA) further revealed the defective motility of BBOF1-deleted spermatozoa (Fig. 2J–L; Supplementary Fig. 3B–E). Capacitation was seen in both WT and BBOF1-deleted sperms. Therefore, BBOF1 deletion led to typical asthenozoospermia with reduced motility but with a normal morphology.

To understand the underlying mechanisms of subfertility, we superovulated WT females and mated them with adult WT or *Bbof1*$^{-/-}$ males. The majority of embryos from females mated with WT males exhibited a normal morphology at the 2-cell stage (40 h after hCG administration). However, only a few embryos/oocytes from females mated with *Bbof1*$^{-/-}$ males were fertilized (1 of 137). Spindle and F-actin staining showed that most embryos were arrested at the MII stage with intact spindles and condensed chromosomes, i.e., not fertilized (Fig. 3A–C).

The subfertility of *Bbof1*$^{-/-}$ males could be attributed to obstructive azoospermia, in which the vas deferens, epididymis, and ejaculatory ducts are obstructed, or asthenozoospermia, where sperm motility is insufficient for MII oocyte fertilization. We performed in vitro fertilization (IVF) experiments to rule out the possibility of ductal obstruction. Spermatozoa obtained from the *Bbof1*$^{-/-}$ and WT cauda epididymides were incubated with WT cumulus-oocyte complexes (COCs) for IVF. In comparison with the WT group, in which most oocytes were successfully fertilized (24 h post-hCG administration), oocytes in the *Bbof1*$^{-/-}$ group failed to fertilize and remained at the MII stage (Fig. 3D–F, ZP-intact). Only a small proportion of oocytes (20 of 436; 4.59%) were fertilized with BBOF1-null spermatozoa and developed to the 2-cell stage, which is consistent with the subfertility of males observed during fertility test (Supplementary Movie 3 and 4).

In *Xenopus*, bbof1 has been reported to be associated with motile cilia. Considering that the sperm flagellum is a specialized type of motile cilium and that *Bbof1* is specifically expressed in the testes, we hypothesized that mammalian BBOF1 functions mainly in the sperm flagellum and is exclusively required for sperm motility. In IVF experiments, spermatozoa should interact with and penetrate the zona pellucida, a thick layer of gel-like glycoprotein surrounding oocytes, which requires sufficient capacitation and motility. When zona pellucida was removed with acidic medium, MII oocytes were comparably fertilized with WT and BBOF1-null spermatozoa (96.9% vs. 92.5%, P = 0.25) (Fig. 3D–F, ZP-free), suggesting reduced motility of BBOF1-null spermatozoa.

BBOF1 is required for axonemal assembly in the sperm flagellum

Sperm motility relies largely on an intact flagellar structure. Therefore, we investigated the ultrastructure of WT and BBOF1-deleted sperm flagella by transmission electron microscopy (TEM). In the mid-piece, BBOF1-deleted spermatozoa had an intact "9 + 2" axonemal structure with intact MTDs, radial spokes, dynein arms, as well as ODFs. However, the absence of one to three MTD(s) was frequently observed in the principal piece and end piece (Fig. 4A; Supplementary Fig. 4). Abnormal axonemes accounted for approximately 30–40% of all cross-sections of the principal piece and end piece (Fig. 4B). Based on statistical analysis, MTD-1, 2, 7, 9, or their combinations were likely to be absent, as indicated by the representative images (Fig. 4A and C). MTD-9, MTD-1, and MTD-7/9 were the top three most frequently absent MTDs (Fig. 4C). Together with the absence of MTDs, the corresponding ODFs were often missing (Fig. 4A), suggesting the role of BBOF1 in the maintenance of the sperm flagellar ultrastructure.

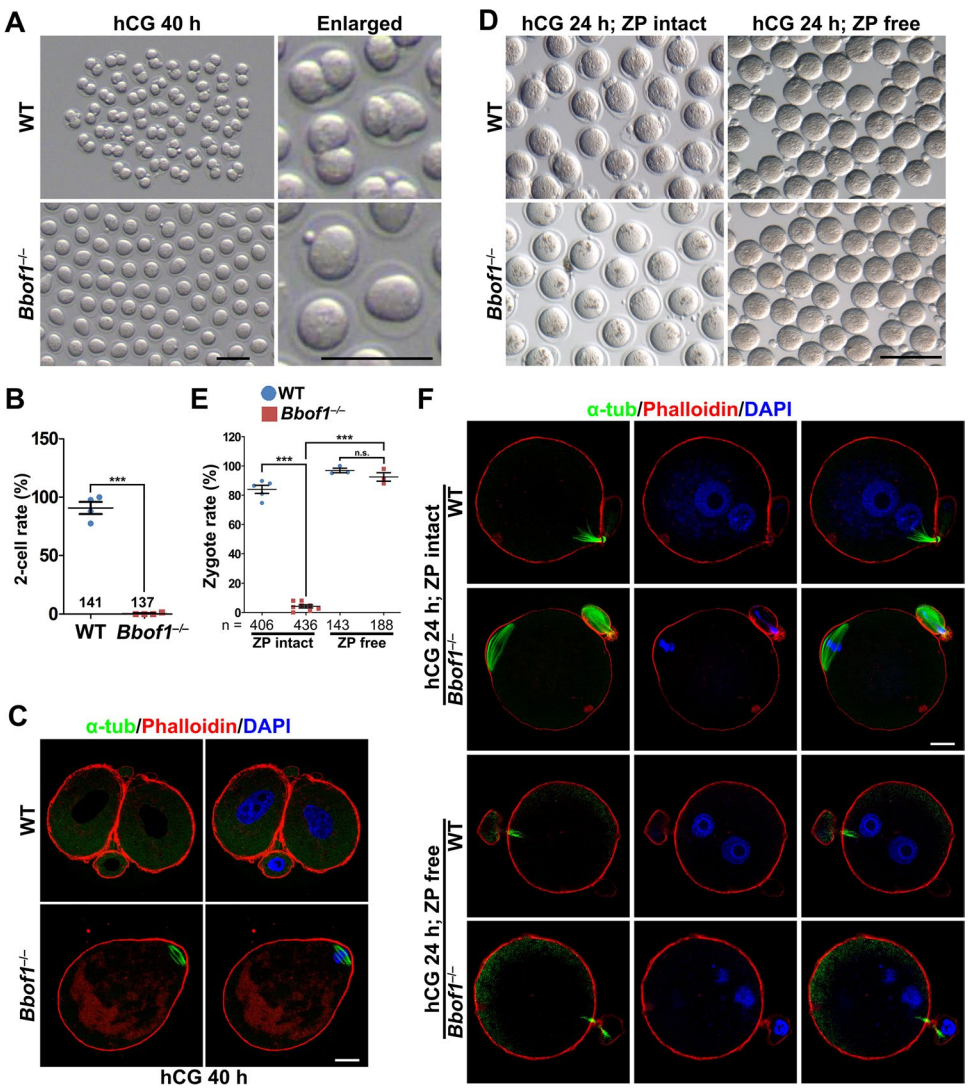

Fig. 3 BBOF1-deleted spermatozoa fail to fertilize mature MII oocytes due to decreased motility. **A** Representative images of embryos from superovulated WT females mated with adult WT or *Bbof1*$^{-/-}$ males. $n=4$ pairs of mice in each experimental group. Scale bars, 100 μm. **B** Rates of embryos at the 2-cell stage in (**A**). The numbers of embryos analyzed are indicated. Error bars indicate the S.E.M. $***P<0.001$ (two-tailed Student's *t*-test). **C** Co-staining of α-tubulin (green) and phalloidin (red) with DAPI (blue) in 2-cell embryos from WT females mated with WT or *Bbof1*$^{-/-}$ males. Scale bar, 10 μm. **D** Morphology of embryos in IVF experiments with spermatozoa from adult WT or *Bbof1*$^{-/-}$ males. ZP, zona pellucida. Scale bar, 100 μm. **E** Rates of oocytes fertilized in (**D**). The numbers of embryos analyzed are indicated. Error bars indicate the S.E.M. $***P<0.001$; n.s., not significant (two-tailed Student's *t*-test). **F** Co-staining of α-tubulin (green), phalloidin (red) and DAPI (blue) in embryos from IVF experiments. Scale bar, 10 μm

BBOF1 interacts with MNS1 and ODF2

To elucidate the molecular functions of BBOF1 in axonemal assembly in the sperm flagellum, yeast two-hybrid (Y2H) screening was performed to identify BBOF1-interacting proteins. Full-length mouse BBOF1 (aa 1–533) was fused to Gal4-BD as the bait protein. The Gal4-AD plasmid library carrying the total PD30 testis cDNA was used for large-scale screening. Combining the results of two rounds of screening, 1014 positive colonies and 52 BBOF1-interacting candidates were sorted and listed based on the number of colonies identified (Fig. 5A, only candidates interacting at least twice are shown). The top four candidates were SPATA24, RP9, MNS1, and ODF2, among which MNS1 is an axonemal component, and ODF2 is an ODF component (Supplementary Fig. 5A–B). The minimal BBOF1-interacting regions of the four candidates were identified based on the cDNA fragments of AD plasmids from positive colonies (Supplementary Fig. 5A).

BBOF1 is identified as a CCDC protein (CCDC176) with two conserved coiled-coil domains on its N-terminal (aa 81–195) and C-terminal (aa 277–366) domains (Fig. 5B). Domain mapping results demonstrated that the C-terminal domain of BBOF1 could mediate its interaction with various proteins, such as ODF2, MNS1, SPATA24, RP9, and IFT74 (Fig. 5C–D; Supplementary Fig. 5). However, in some cases, the whole sequence of BBOF1 was required, such as during the interaction with SASS6, CFAP57, and CCDC136 (Supplementary Fig. 5). Notably, the putative mutant protein BBOF1-KO expressed in *Bbof1*$^{-/-}$ mice could not bind to all of the examined BBOF1 interactors (Fig. 5C–D; Supplementary Fig. 5).

Y2H analysis revealed that BBOF1 could interact with sperm tail-specific proteins, including the axonemal component MNS1 and outer dense fiber proteins ODF2, suggesting the possible role of BBOF1 in mediating the association between ODFs and the axoneme. Therefore, we investigated whether BBOF1 deletion affects

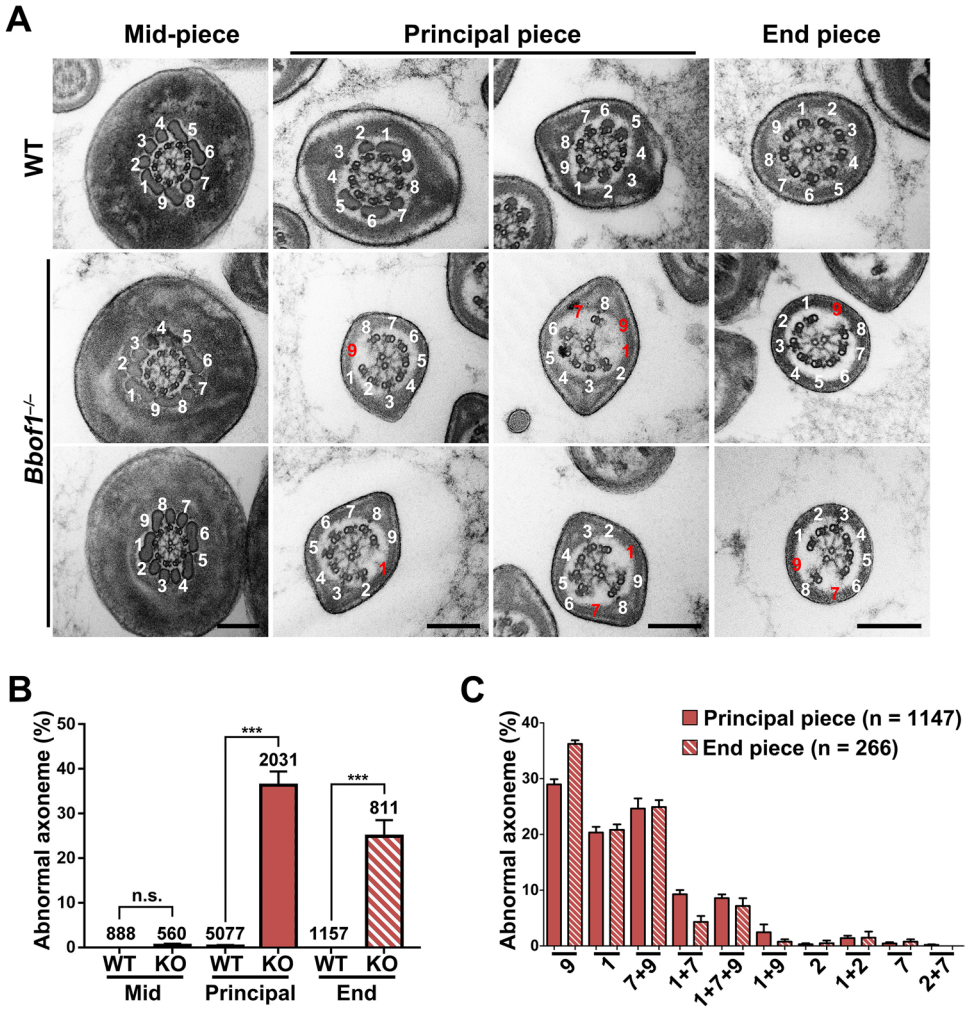

Fig. 4 BBOF1 deletion results in abnormalities in sperm flagellar axoneme. **A** Representative images of the cross-sections of mid-piece, principal piece and end piece from TEM of the ultrastructure of WT and *Bbof1*$^{-/-}$ sperm flagella. Typical order of well-arranged MTDs are indicated by numbers in white, whereas absent MTDs and ODFs are indicated by numbers in red. Scale bars, 200 nm. **B** Quantification of abnormal axonemes (with certain MTDs absent) in mid-piece, principal piece and end piece in WT and *Bbof1*$^{-/-}$ spermatozoa. Numbers of cross-sections analyzed are indicated above the corresponding bars. Error bars indicate the S.E.M. ***, $P < 0.001$; n.s., not significant (two-tailed Student's *t*-test). **C** Quantification of the frequency of cross-sections with the indicated absent MTD combinations in principal piece and end piece of *Bbof1*$^{-/-}$ spermatozoa. The numbers of cross-sections analyzed (*n*) are indicated. Error bars indicate the S.E.M

the stability and localization of MNS1 and ODF2. In *Bbof1*$^{-/-}$ mouse testes, the endogenous protein levels of ODF2 and MNS1 were decreased (Fig. 6A), indicating that BBOF1 is required for the stabilization of ODF2 and MNS1. However, the localization of MNS1 and ODF2 in the sperm flagellum was not affected by BBOF1 deletion (Fig. 6B–C). Furthermore, we lysed WT and BBOF1-deleted spermatozoa to give rise to three protein fractions: Triton X-100-soluble (TS), SDS-soluble (SS), and SDS-resistant (SR), representing cytosolic or membrane-associated proteins, axonemal proteins and accessory structures in flagella (composed of ODFs, fibrous sheath and mitochondrial sheath), respectively. Similar to MNS1, BBOF1 was detected mainly in the SS fraction and partially in the SR fraction from WT spermatozoa (Fig. 6D). However, the protein level of MNS1 was markedly decreased in the SS fraction from BBOF1-deleted spermatozoa. Moreover, ODF2 was detected in the SR fraction from both WT and BBOF1-deleted spermatozoa and its level was decreased in BBOF1-deleted spermatozoa (Fig. 6D). These results suggested that BBOF1 may preferentially localize to the axonemal structure and may be required for the stability of MNS1 and ODF2.

BBOF1 is dispensable for the function of motile cilia

As the "9 + 2" axonemal structure is commonly found in all types of motile cilia, we further investigated whether subfertility is a symptom of PCD. *Bbof1*$^{-/-}$ mice did not show typical PCD symptoms, such as hydrocephalus, respiratory tract infections, or ectopic positioning of internal organs (situs inversus) during breeding, fertility testing, and maintenance (Supplementary Fig. 1). Brain samples obtained from *Bbof1*$^{-/-}$ mice exhibited a normal external morphology (Fig. 7A), and the ventricles were not enlarged, as observed in the tissue sections (Fig. 7B). The differentiation of ependymal cells and motile cilia on their surface were not affected by BBOF1 deletion (Fig. 7C–D; Supplementary Fig. 6A). Similarly, motile cilia were normally distributed on the epithelial cells of the trachea of *Bbof1*$^{-/-}$ mice (Fig. 7E–F; Supplementary Fig. 6B). We also examined the ultrastructure of the tracheal cilia and found that the axonemal structure was

A

Interactor	Count
SPATA24	129
RP9	78
ODF2	76
MNS1	72
SFR1	48
GKAP1	39
CIR1	15
CCDC158	10
SASS6	9
HIPK3	8
SUDS3	7
GTSF1L	6
UBE2I	6
IFT74	4
CFAP57	4
HGS	4
PIAS4	4
DNAJB7	4
LYAR	3
TGFB1I1	3
NCOA5	3
CCDC136	2

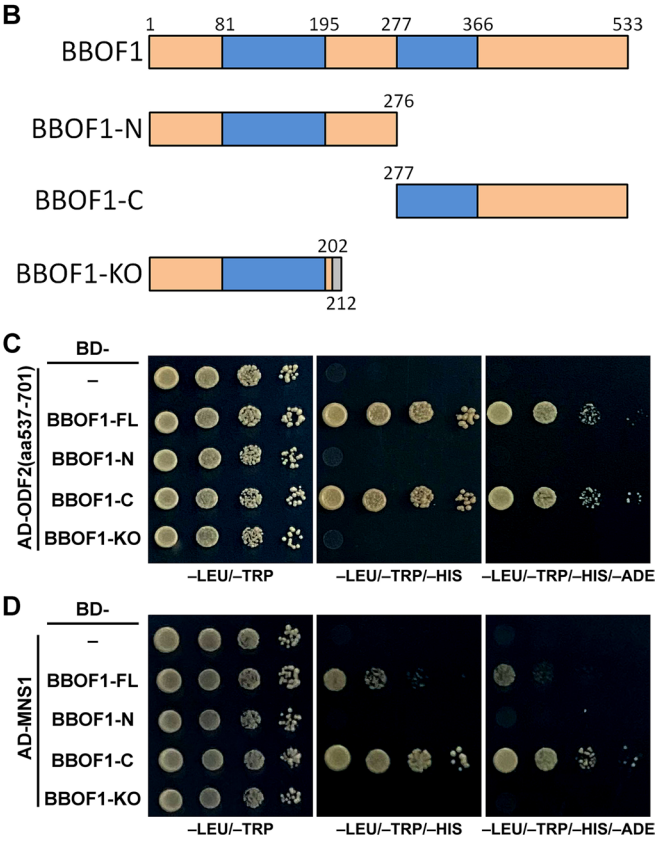

Fig. 5 MNS1 and ODF2 are BBOF1 interactors. **A** Summary of BBOF1-interacting candidates and the corresponding number of colonies identified by yeast-two-hybrid (Y2H) screening. Interactors identified more than once are listed. **B** Schematic diagram of BBOF1 and its truncations or mutations. BBOF1-KO is the 212-aa putative protein product expressed in *Bbof1*$^{-/-}$ mice. The lengths of the amino acid sequences are indicated. The positions of the coiled-coil domains are indicated in blue. **C–D** Y2H analysis on the interaction of truncated ODF2 (**C**) or MNS1 (**D**) with the full-length (FL) BBOF1 and the C-terminal region of BBOF1

intact in *Bbof1*$^{-/-}$ mouse tracheal sections (Fig. 7G). Notably, although the phenotypes of PCD were not evident in *Bbof1*$^{-/-}$ brain ventricles and tracheas, motile cilia on their surfaces were more curved than WT controls (Fig. 7; Supplementary Fig. 6). Taken together, BBOF1 is dispensable for the assembly and function of motile cilia and thus may play a role in regulating the structural integrity of the sperm flagellum.

Discussion

Here, we identified a novel axoneme-associated protein, BBOF1 in mice, which is predominantly expressed in male germ cells and required for the stabilization of the sperm flagellar ultrastructure. BBOF1 deletion could cause severe defects in axonemal organization, as demonstrated by the absence of certain peripheral MTDs, which is typically observed in the mutations of genes encoding axonemal components [2]. However, in most of these mutants, reduced motility is accompanied by abnormal morphology and decreased sperm count, resulting in varying degrees of oligoasthenoteratozoospermia. Only a few genes have been reported to be exclusively associated with asthenozoospermia. DNAH17 is a dynein axonemal heavy chain protein, and loss-of-function of *DNAH17* causes deficiencies in MTDs 4–7 and consequently asthenozoospermia without adverse effects on sperm count and morphology [38]. Recently, LRRC23, a component of radial spokes, has been reported to be associated with asthenozoospermia [39]. As various factors (lifestyle, drugs, environmental insults, etc.) are also associated with asthenozoospermia, the identification of genetic factors underlying asthenozoospermia is of great significance for accurate diagnosis and effective treatment in clinics. In this study, BBOF1 deletion in mice led to reduced sperm motility and male subfertility without obvious sperm morphological defects, thus demonstrating the importance of genetic factors underlying isolated asthenozoospermia.

The subcellular localization of BBOF1 in spermatozoa could not be determined after immunostaining experiments with several BBOF1 antibodies (both commercial and homemade). Nevertheless, we believe that BBOF1 may be associated with axonemal or peri-axonemal components in the sperm flagella based on the evidence showing the presence of BBOF1 in the SS and SR fractions of spermatozoa composed of proteins that assemble the axoneme and accessory structures, as well as the interaction of BBOF1 with the axoneme-associated protein MNS1 and the ODF component ODF2. Unlike BBOF1, MNS1 is an axonemal protein required for the function of various types of motile cilia, including sperm flagella [49–51]. Previously, mice

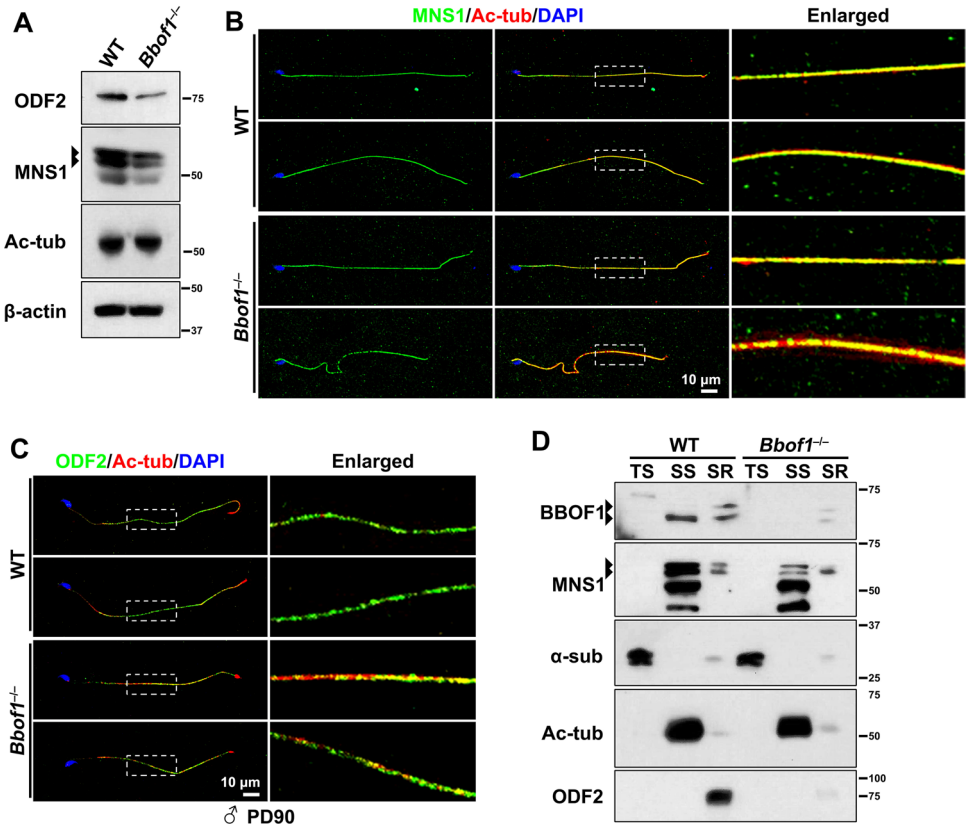

Fig. 6 MNS1 and ODF2 protein levels rather than localization are affected by BBOF1 deletion. **A** Western blotting showing the protein levels of MNS1 and ODF2 in WT and *Bbof1*$^{-/-}$ testes at PD42. MNS1 bands are indicated by arrowheads. β-Actin acts as the loading control. **B**–**C** Immunofluorescence co-staining of MNS1 (**B**, green) or ODF2 (**C**, green) with acetylated α-tubulin (Ac-tub, red) in spermatozoa from WT and *Bbof1*$^{-/-}$ males at PD90. Enlarged images illustrate the fine localization of relative proteins and the enlarged regions are marked with dashed boxes. Scale bars, 10 μm. **D** Western blotting showing the distribution of BBOF1, MNS1, and ODF2 in sperm fractions. The BBOF1 or MNS1 bands are indicated by arrowheads. α-Subunit (α-sub), Ac-tub, and ODF2 are protein markers for their respective fractions (Triton X-100-soluble, SDS-soluble, and SDS-resistant). TS, Triton X-100-soluble; SS, SDS-soluble; SR, SDS-resistant

with MNS1 deficiency have been found to exhibit infertility, mild hydrocephalus, and left/right asymmetry. In MNS1-deleted mice, the "9 + 2" microtubule arrangement and ODFs were disrupted in the sperm flagella, and ODAs were partially absent in the axonemes of the tracheal cilia. ODF2/Cenexin1 is one of the major ODF proteins in sperm flagella and is associated with sperm motility [41, 43, 52, 53]. The axonemal disorganization observed in BBOF1-deleted sperm flagella was consistent with that observed in MNS1- or ODF2-deleted sperm flagella. In addition to the essential role of BBOF1 in the distribution of MNS1 and ODF2 in sperm flagella, it may be required for the stabilization of these proteins. Taken together, the findings suggest that BBOF1 may form a link between ODFs and axonemes and thus facilitate the function of ODFs on axonemal integrity maintenance. However, additional studies are required to further investigate the role of BBOF1 in coupling ODFs and microtubules. For example, the protein structure of BBOF1 could be analyzed to determine its molecular function. In addition, the mechanisms underlying BBOF1 and its interactors, such as RP9 and SPATA24, could be investigated.

According to the present findings, BBOF1 may be dispensable for the function of motile cilia in the brain and trachea. PCD is an inherited disorder caused by defects in motile cilia and is usually characterized by cilia-associated, multisystemic dysfunctions, including respiratory diseases, congenital hydrocephalus, and male infertility [54–56]. Some axoneme-associated proteins have a universal function in all types of motile cilia, including sperm flagella; however, some proteins are flagella-specific [2, 57]. As BBOF1-deficient mice exhibited no apparent developmental defects or cilia-related symptoms such as hydrocephalus, airway infection, and situs inversus, BBOF1 may be a sperm flagella-associated component that specifically participates in the axonemal organization and motility maintenance of sperm flagella. Accordingly, BBOF1 deficiency led to asthenozoospermia and subfertility rather than PCD-related disorders in the mice.

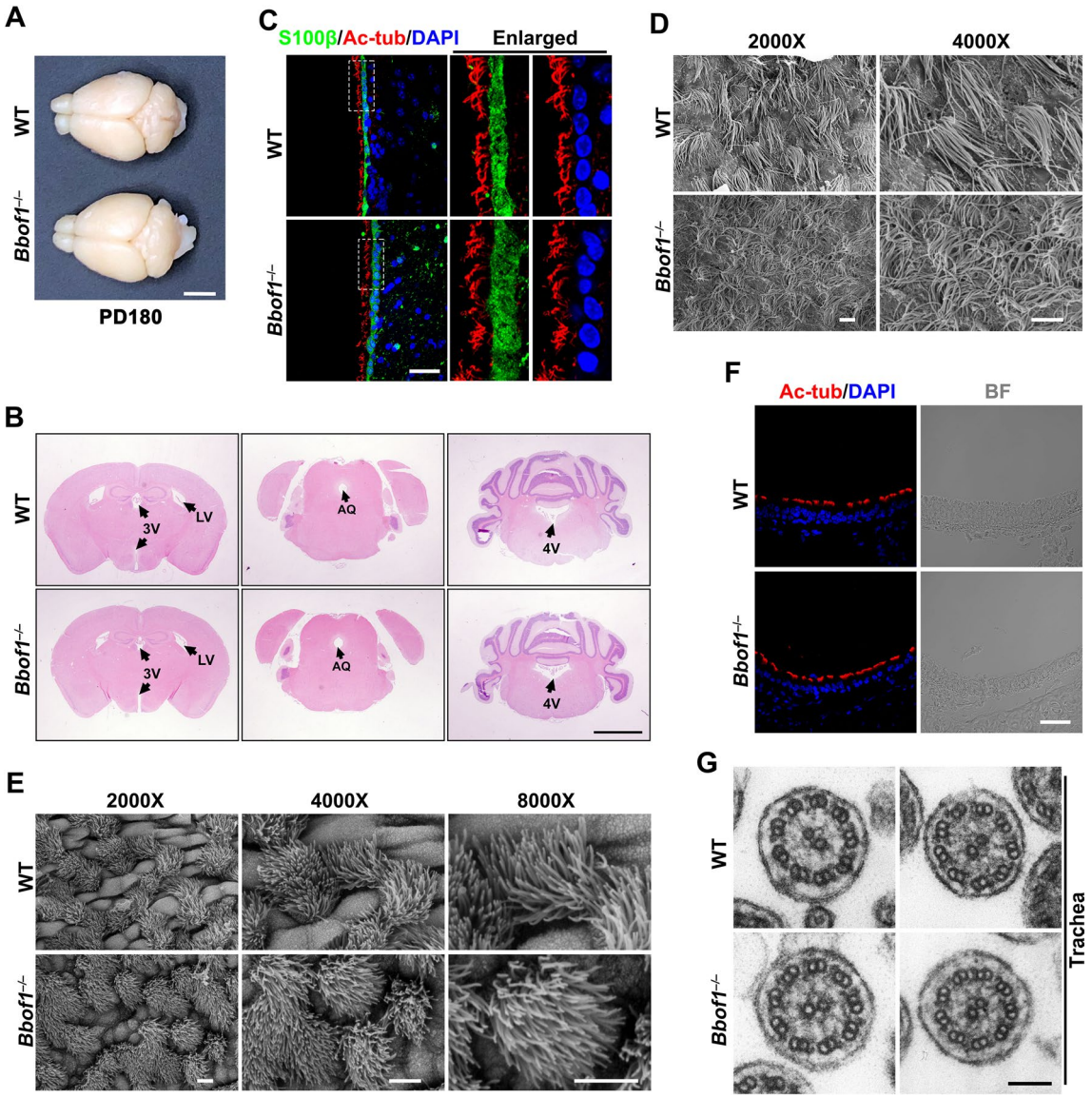

Fig. 7 BBOF1 deletion has compromised effects on brain ependymal cells and tracheal epithelial cells. **A** Representative images of brain samples obtained from WT and *Bbof1*$^{-/-}$ mice at PD180. Scale bar, 0.5 cm. **B** H&E staining of WT and *Bbof1*$^{-/-}$ brain coronal sections. *LV* lateral ventricle, *3 V* third ventricle, *AQ* aqueduct, 4 V, fourth ventricle. Scale bar, 2 mm. **C** Co-staining of S100β (a marker of ependymal cells, green) and acetylated α-tubulin (Ac-tub, red) on brain sections. BF, bright field. Scale bars, 50 μm. **D** Scanning electron microscopy (SEM) images of WT and *Bbof1*$^{-/-}$ ependymal cilia on the surface of brain lateral ventricles. Scale bars, 50 μm. **E** SEM images of WT and *Bbof1*$^{-/-}$ tracheal epithelia. Scale bars, 50 μm. **F** Immunofluorescence staining of acetylated α-tubulin (Ac-tub, red) on tracheal cross-sections derived from WT and *Bbof1*$^{-/-}$ mice. Scale bar, 50 μm. **G** TEM images of the cross-sections of WT and *Bbof1*$^{-/-}$ tracheal cilia. Scale bar, 100 nm

The hypoexpression of ODF proteins or MNS1 variants has been found to genetically contribute to male infertility in humans [58–61]. However, we have not detected *BBOF1* mutations in patients with asthenozoospermia, which might be attributed to the varied and complex etiology of asthenozoospermia in clinics. Interestingly, *Bbof1*-knockout males showed residual fertility, as demonstrated by the pups born during fertility test and the recovery of zygotes/2-cell embryos from IVF experiments, suggesting that BBOF1-deleted spermatozoa could support embryo development without further defects. Currently, intracytoplasmic sperm injection (ICSI) is the most efficient clinical strategy for patients with asthenozoospermia to achieve pregnancy. Despite the widespread success of ICSI, there is a risk of transmission of pathological genetic variations to the next generation. Therefore, understanding the etiology of asthenozoospermia would benefit patients in terms

of accurate diagnosis and genetic screening before ICSI and eventually improve the quality of embryos.

Methods

Mice

Heterogeneous *Bbof1* (*Bbof1*$^{+/-}$) mouse stain (C57BL/6), which was generated via CRISPR/Cas9 technology, was purchased from GemPharmatech LLC. The knockout strategy and sgRNA sequence used were described in Fig. 1D. The genomic DNA of founder mice have been examined by PCR and sequencing to verify the mutation of *Bbof1* gene. *Bbof1*$^{+/-}$ mice have been crossed with WT mice for three consecutive generations to eliminate possible off-targeting effects. All mutant mouse strains had a C57BL/6 background. The genotyping primers are listed in Supplementary Table 1. All mice were housed under standard SPF conditions (20–22 °C, 12 h light/dark cycle, 50–70% humidity, adequate food/water supply). The experimental procedures were approved by the Zhejiang University Institutional Animal Care and Research Committee, and mouse care was performed in accordance with the relevant guidelines and regulations of Zhejiang University.

Fertility test

For male fertility test, adult *Bbof1*$^{-/-}$ males and their *Bbof1*$^{+/-}$ littermates were crossed with two 8-week-old *Bbof1*$^{+/-}$ females, respectively. For female fertility test, 8-week-old *Bbof1*$^{-/-}$ females were crossed with adult *Bbof1*$^{+/-}$ males. The breeding was maintained consecutively for at least 3 months. During the duration of fertility test, vaginal plugs were checked every morning. The presence of vaginal plugs, pregnancy, and number of pups born were recorded to calculate the number of pups per plug and pups per litter.

Superovulation and embryo assay

Wildtype (WT) pubertal female mice (21–23 days old) were superovulated by successive intraperitoneal injection of 5 IU PMSG and 5 IU hCG (Sansheng Pharmaceutical, Ningbo, China) with a time interval of 44–48 h, and immediately mated with WT or *Bbof1*$^{-/-}$ males upon hCG administration. Vaginal plugs were checked in the next morning as a sign of successful mating. The females were sacrificed at 24 h or 40 h post-hCG administration to collect 1-cell or 2-cell embryos, respectively. The embryo images were acquired with Nikon SMZ745T stereoscope. For immunofluorescent staining, oocytes and embryos were fixed in 4% PFA. After permeabilization with 0.2% triton X-100, samples were incubated with rhodamine-conjugated phalloidin, to stain F-actin, and FITC-conjugated α-tubulin antibody, to stain spindles.

In vitro fertilization (IVF)

Superovulation processes for MII oocytes are the same as described above. On the day of IVF, cauda epididymides and vas deferens were dissected and placed in HTF medium to recover spermatozoa. Cumulus-oocyte complexes (COCs) were collected from superovulated WT females at 16 h post-hCG administration. COCs were incubated with 1 mg/ml hyaluronidase for 1 min to remove the cumulus cells and with acidic M2 medium (pH 2.0, adjusted with HCl) to remove the zona pellucida. After incubation in HTF medium for 1 h, WT and *Bbof1*$^{-/-}$ spermatozoa were added to the COCs, ZP-intact or ZP-free oocytes. 6 h after IVF, oocytes/zygotes were washed and transferred to KSOM medium for further embryogenesis.

Isolation of male germ cells

Individual populations of male germ cells at different developmental stages were isolated by testis dissociation, followed by Hoechst-33342-based FACS (fluorescence-activated cell sorting) with BD Influx™ Cell Sorter. Briefly, seminiferous tubules were incubated in PBS containing collagenase type I at 32 °C, followed by trypsin digestion. After termination of digestion by adding FBS and filtration through a 70 μm cell strainer, cells were resuspended and stained with Hoechst 33,342 for 30 min at 32 °C. Dead cells were excluded by propidium iodide (PI) staining immediately prior to sorting.

Semi-quantitative RT-PCR

Tissues were dissected from adult mice. Germ cells were isolated by FACS. Total RNA was purified from cells and tissues with RNeasy Mini Kit (Qiagen, Cat. 74,104), and cDNA was synthesized with PrimeScript™ II 1st Strand cDNA Synthesis Kit (TaKaRa, 6210A). Semi-quantitative PCR were carried out with 2X Taq DNA Polymerase Mix following standard procedures for 22–30 cycles. The PCR primers designed for amplifying *Bbof1* and *Gapdh* fragments are listed in Supplementary Table 1.

Western blotting

Total testis proteins were extracted and denatured in SDS loading buffer (25 mM Tris–HCl [pH 6.8], 2% SDS, 10% glycerol, 5% β-mercaptoethanol, 0.01% bromophenol blue), assisted with thoroughly sonication. For protein fractionation assay, spermatozoa were initially lysed with cell lysis buffer (25 mM Tris–HCl [pH 7.5], 300 mM NaCl, 1%

Triton X-100, 1 mM DTT, 1 mM PMSF) and centrifuged at 15,000 g for 10 min. The supernatant was defined as Triton X-100-soluble fraction (TS). The pellet was resuspended in cell lysis buffer with 1% SDS and centrifuged at 15,000 g for 10 min. The resulting supernatant and pellet contained SDS-soluble (SS) and SDS-resistant (SR) fractions, respectively. Same volumes of all three fractions were subjected to Western blotting. Protein samples were separated by SDS–polyacrylamide gel electrophoresis, and transferred to PVDF membrane with semi-dry transfer device (Bio-Rad). After sequentially incubated with diluted primary antibody and HRP-conjugated secondary antibodies (Jackson ImmunoResearch), signals were developed with SuperSignal™ West Pico PLUS (Thermo Fisher, Cat. 34,577) and images were taken with Odyssey® Fc Imaging System. The antibodies used are listed in Supplementary Table 2. Unprocessed images of Western blotting are provided in Supplementary Fig. 7.

Histological analyses

Bbof1$^{-/-}$ males and their male littermates were examined and weighted once a week since PD7. Adult WT and *Bbof1*$^{-/-}$ males were sacrificed for phenotype analyses. Testes, brains and tracheas were dissected and imaged. For H&E staining of testes and epididymides, samples were fixed in Bouin's solution, and for other histological analyses and immunofluorescent staining, samples were fixed in PBS buffered 3.7% formaldehyde. After fixation, tissues were dehydrated with an ethanol gradient and xylene, and finally embedded in paraffin. 5 μm-thick cross-sections were prepared afterwards. For H&E staining, paraffin-embedded sections were deparaffinized, rehydrated and sequentially stained with hematoxylin and eosin respectively for 30–60 s.

Immunofluorescent staining (IF)

Paraffin-embedded sections were deparaffinized and rehydrated through xylene and ethanol gradient. Afterwards, the slides were incubated in blocking buffer (1% BSA in PBS with 0.1% Tween-20) for 30 min, diluted primary antibody for 1 h, diluted Fluorophores (FITC and CY3)-conjugated secondary antibody (Jackson ImmunoResearch) for 30 min, and 5 μg/mL DAPI for 10 min. The stained slides were mounted and imaged with a confocal laser scanning microscope (Olympus, FV3000). The antibodies involved are listed in Supplementary Table 2.

Sperm assay

Spermatozoa isolated from the cauda epididymides of *Bbof1*$^{-/-}$ males and their littermates were cultured in either PBS or human tubal fluid (HTF) containing 10% FBS. The sperm concentration was measured by hemocytometer and the movement was recorded at 100 frames/second by Nikon eclipse 80i microscope equipped with high-speed camera. The motility of spermatozoa was assessed with a computer-assisted sperm analysis (CASA) system at 1 h after incubation in PBS or HTF medium, and at least 400 sperms were analyzed for each sample. Spermatozoa suspension were spread on adhesive microscopy slides, air-dried, successively fixed in 4% PFA and subjected to Papanicolaou staining (Solarbio) or immunofluorescent staining.

Transmission electron microscopy (TEM)

Cauda epididymides and tracheas were initially processed with double fixation procedure. The detailed process is as follows: fixed with 2.5% glutaraldehyde (diluted in 0.1 M phosphate buffer [pH 7.0]) for over 4 h; washed thoroughly in PBS for three times and 15 min each time; fixed with 1% OsO4 in PBS for 1–2 h and washed again. The fixed samples were serially dehydrated by an ethanol gradient (30%, 50%, 70%, 80%) and an acetone gradient (90%, 95%, 100%, 100%) for 15–20 min at each step. Later, the samples were sequentially infiltrated in a mixture of Spurr resin and acetone (V/V = 1/1) for 1 h, a mixture of Spurr resin and acetone (V/V = 1/3) for 3 h and absolute Spurr resin for overnight, followed by embedding in Spurr resin at 70 °C for overnight, ultrathin sectioning in LEICA EM UC7 ultratome and staining with alkaline lead citrate solution and uranyl acetate (saturated solution in 50% ethanol) for 5–10 min, respectively. Finally, specimens were imaged with Hitachi Model H-7650 TEM or JEOL 2100 plus TEM (JEOL, Tokyo, Japan). The complete process was conducted in Bio-ultrastructure Analysis Laboratory of Analysis Center of Agrobiology and Environmental sciences, Zhejiang University.

Scanning electron microscopy (SEM)

Sample processing procedures for SEM are similar to TEM. Briefly, samples were first fixed with 2.5% glutaraldehyde and for 1 h and post-fixed with 1% OsO_4 in phosphate buffer (0.1 M, pH 7.0) for 1 h at room temperature. After double fixation, samples were dehydrated through a graded series of ethanol solutions. After dehydration in Hitachi Model HCP-2 critical point dryer, samples were coated with gold–palladium in Hitachi Model E-1010 ion sputter for 4–5 min. The samples were finally scanned under a Hitachi Model SU-8010 SEM.

cDNA cloning

cDNAs encoding *Bbof1*, *Mns1*, *Odf2*, *Rp9* and *Spata24* were PCR amplified from mouse testes cDNA and cloned into

pGBKT7 (Bait) or pGADT7 (Prey) vectors for yeast-two-hybrid assay.

Yeast-two-hybrid (Y2H)

Host strain AH109, empty vectors pGBKT7, pGADT7 as well as AD Fusion Plasmid Library (AD/Library, 1×10^6 independent clones) established with cDNA from PD30 mouse testes were purchased from Shanghai Hitech Bio-Technology Co., Ltd. Y2H screening and Two-hybrid analysis were carried out according to the Matchmaker™ GAL4 Two-Hybrid System 3 & Libraries User Manual (Clontech Laboratories, Inc.). Yeast transformation was conducted through the polyethylene glycol/lithium acetate (PEG/LiAc) strategy. AH109 cells were initially transformed with pGBKT7-BBOF1 (BD-BBOF1) and selected on SD/–Trp plate. Colonies carrying BD-BBOF1 were amplified for library transformation and screening. Transformation efficiency was analyzed by serial-dilutions (1:10, 1:100, 1:1000) on SD/–Trp–Leu plates. Candidate colonies were recovered on SD/–Trp–Leu–His agar plates. After incubation at 30 °C 5–7 days, transformation efficiency was calculated and colonies screened were transferred on SD/–Trp–Leu–His–Ade high-stringency plates for secondary screening. Plasmids were isolated from positive colonies with Yeast Plasmid Extraction Kit (Solarbio, D1160) and cDNA fragments were amplified, sequenced and analyzed with BLASTn to identify BBOF1-interacting candidates. For further verification, full-length cDNA and functional domains of candidates such as MNS1 and ODF2 were cloned into pGADT7 (AD-pray). The yeast stains containing BD-BBOF1 and AD-pray were serial-diluted and cultured on SD/–Trp–Leu–His and SD/–Trp–Leu–His–Ade plates as dot plots. 2–3 days later, positive colonies were observed and images of plates were obtained with cell phone.

Statistical analysis

For each experiment, at least three independent experiments were carried out with similar results. The statistical data were processed and exhibited as means ± S.E.M. The significance of differences between two independent groups was analyzed by two-tailed unbiased Student's *t* test.

Supplementary Information The online version contains supplementary material available at https://doi.org/10.1007/s00018-023-04800-0.

Acknowledgements We thank Heng-Yu Fan (Zhejiang University) for discussions and Dr. Fei Sun (Sir Run Run Shaw Hospital, Zhejiang University) for the ODF2 antibody. We also thank for the technical support by the Core Facility, Zhejiang University-University of Edinburgh Institute.

Author contributions C.Y. and Q.Z designed the project. C.Y., Q.Z., H.C. and H.X. performed the experiments and analyzed the data. W.X. and Q.L. performed the isolation of male germ cells and fractionation of sperm components. Y.Z. performed the yeast-2-hybrid. Y.Z. and H.C. did mouse breeding. L.J. and Y.R. analyzed mouse sperm samples. Q.Z. and C.Y. wrote the manuscript with help from all the authors. All the authors read and approved this manuscript.

Funding This work is supported by National Natural Science Foundation of China (82171598 and 32222029 to C.Y.; 82271380 and 32200671 to Q.Z.), and Zhejiang Provincial Natural Science Fund (LR21C120001 to C.Y. and LQ21C050002 to Q.Z.).

Data availability The authors declare that all the original data related to the figures and supplementary materials published in this article are available upon rationale request to the corresponding author.

Availability of data and material All related data are included in either the manuscript or supplementary information.

Declarations

Competing interests The authors declare no competing interests.

Ethics approval and consent to participate Not applicable.

Consent for publication The author's consent to publication.

References

1. Hosseinzadeh Colagar A, Karimi F (2014) Large scale deletions of the mitochondrial DNA in astheno, asthenoterato and oligoasthenoterato-spermic men. Mitochondrial DNA 25:321–328
2. Toure A et al (2021) The genetic architecture of morphological abnormalities of the sperm tail. Hum Genet 140:21–42
3. El-Kamshoushi AM, Zohdy NI, Abou Khedr NA, Nabhan SA, Mostafa T (2013) Ultrastructure of the seminiferous tubules in oligoasthenoteratozoospermic men associated with varicocele. Andrologia 45:319–325
4. Organization WH (2021) WHO Laboratory Manual for the Examination and Processing of Human Semen, 6th edn. World Health Organization, Geneva
5. Gole LA et al (2001) Does sperm morphology play a significant role in increased sex chromosomal disomy? A comparison between patients with teratozoospermia and OAT by FISH. J Androl 22:759–763
6. Ben Khelifa M et al (2014) Mutations in DNAH1, which encodes an inner arm heavy chain dynein, lead to male infertility from multiple morphological abnormalities of the sperm flagella. Am J Hum Genet 94:95–104
7. Li Y et al (2019) DNAH2 is a novel candidate gene associated with multiple morphological abnormalities of the sperm flagella. Clin Genet 95:590–600
8. Tu C et al (2019) Identification of DNAH6 mutations in infertile men with multiple morphological abnormalities of the sperm flagella. Sci Rep 9:15864
9. Olbrich H et al (2002) Mutations in DNAH5 cause primary ciliary dyskinesia and randomization of left-right asymmetry. Nat Genet 30:143–144
10. Liu C et al (2020) Bi-allelic DNAH8 variants lead to multiple morphological abnormalities of the sperm flagella and primary male infertility. Am J Hum Genet 107:330–341
11. Fassad MR et al (2018) Mutations in outer dynein arm heavy chain DNAH9 cause motile cilia defects and situs inversus. Am J Hum Genet 103:984–994

12. Sha Y et al (2020) DNAH17 is associated with asthenozoospermia and multiple morphological abnormalities of sperm flagella. Ann Hum Genet 84:271–279
13. Guichard C et al (2001) Axonemal dynein intermediate-chain gene (DNAI1) mutations result in situs inversus and primary ciliary dyskinesia (Kartagener syndrome). Am J Hum Genet 68:1030–1035
14. Loges NT et al (2008) DNAI2 mutations cause primary ciliary dyskinesia with defects in the outer dynein arm. Am J Hum Genet 83:547–558
15. Beurois J et al (2019) CFAP70 mutations lead to male infertility due to severe astheno-teratozoospermia. A case report. Hum Reprod 34:2071–2079
16. Liu W et al (2019) Loss-of-function mutations in SPEF2 cause multiple morphological abnormalities of the sperm flagella (MMAF). J Med Genet 56:678–684
17. He X et al (2020) Bi-allelic loss-of-function variants in CFAP58 cause flagellar axoneme and mitochondrial sheath defects and asthenoteratozoospermia in humans and mice. Am J Hum Genet 107:514–526
18. Wang W et al (2019) Biallelic mutations in CFAP65 lead to severe asthenoteratospermia due to acrosome hypoplasia and flagellum malformations. J Med Genet 56:750–757
19. Wu H et al (2020) Patients with severe asthenoteratospermia carrying SPAG6 or RSPH3 mutations have a positive pregnancy outcome following intracytoplasmic sperm injection. J Assist Reprod Genet 37:829–840
20. Martinez G et al (2020) Biallelic variants in MAATS1 encoding CFAP91, a calmodulin-associated and spoke-associated complex protein, cause severe astheno-teratozoospermia and male infertility. J Med Genet 57:708–716
21. Li W et al (2019) Biallelic mutations of CFAP251 cause sperm flagellar defects and human male infertility. J Hum Genet 64:49–54
22. Kott E et al (2013) Loss-of-function mutations in RSPH1 cause primary ciliary dyskinesia with central-complex and radial-spoke defects. Am J Hum Genet 93:561–570
23. Jeanson L et al (2015) RSPH3 mutations cause primary ciliary dyskinesia with central-complex defects and a near absence of radial spokes. Am J Hum Genet 97:153–162
24. Castleman VH et al (2009) Mutations in radial spoke head protein genes RSPH9 and RSPH4A cause primary ciliary dyskinesia with central-microtubular-pair abnormalities. Am J Hum Genet 84:197–209
25. Sha YW et al (2017) A homozygous CEP135 mutation is associated with multiple morphological abnormalities of the sperm flagella (MMAF). Gene 633:48–53
26. Lv M et al (2020) Homozygous mutations in DZIP1 can induce asthenoteratospermia with severe MMAF. J Med Genet 57:445–453
27. Tang S et al (2017) Biallelic mutations in CFAP43 and CFAP44 cause male infertility with multiple morphological abnormalities of the sperm flagella. Am J Hum Genet 100:854–864
28. Coutton C et al (2018) Mutations in CFAP43 and CFAP44 cause male infertility and flagellum defects in Trypanosoma and human. Nat Commun 9:686
29. Liu C et al (2021) Deleterious variants in X-linked CFAP47 induce asthenoteratozoospermia and primary male infertility. Am J Hum Genet 108:309–323
30. Antony D et al (2013) Mutations in CCDC39 and CCDC40 are the major cause of primary ciliary dyskinesia with axonemal disorganization and absent inner dynein arms. Hum Mutat 34:462–472
31. Jeanson L et al (2016) Mutations in GAS8, a gene encoding a nexin-dynein regulatory complex subunit, cause primary ciliary dyskinesia with axonemal disorganization. Hum Mutat 37:776–785
32. Tu C et al (2020) Genetic underpinnings of asthenozoospermia. Best practice and research. Clin Endocrinol Metabol 34:101472
33. Kott E et al (2012) Loss-of-function mutations in LRRC6, a gene essential for proper axonemal assembly of inner and outer dynein arms, cause primary ciliary dyskinesia. Am J Hum Genet 91:958–964
34. Thomas L et al (2020) TTC12 loss-of-function mutations cause primary ciliary dyskinesia and unveil distinct dynein assembly mechanisms in motile cilia versus flagella. Am J Hum Genet 106:153–169
35. Liu W et al (2019) Bi-allelic mutations in TTC21A induce asthenoteratospermia in humans and mice. Am J Hum Genet 104:738–748
36. Liu C et al (2019) Bi-allelic mutations in TTC29 cause male subfertility with asthenoteratospermia in humans and mice. Am J Hum Genet 105:1168–1181
37. Dong FN et al (2018) Absence of CFAP69 causes male infertility due to multiple morphological abnormalities of the flagella in human and mouse. Am J Hum Genet 102:636–648
38. Zhang B et al (2020) A DNAH17 missense variant causes flagella destabilization and asthenozoospermia. J Experim Med. https://doi.org/10.1084/jem.20182365
39. Zhang X et al (2021) LRRC23 is a conserved component of the radial spoke that is necessary for sperm motility and male fertility in mice. J Cell Sci. https://doi.org/10.1242/jcs.259381
40. Lindemann CB, Lesich KA (2016) Functional anatomy of the mammalian sperm flagellum. Cytoskeleton (Hoboken) 73:652–669
41. Pletz N et al (2013) Transcriptional activation of Odf2/Cenexin by cell cycle arrest and the stress activated signaling pathway (JNK pathway). Biochem Biophys Acta 1833:1338–1346
42. Hoyer-Fender S, Petersen C, Brohmann H, Rhee K, Wolgemuth DJ (1998) Mouse Odf2 cDNAs consist of evolutionary conserved as well as highly variable sequences and encode outer dense fiber proteins of the sperm tail. Mol Reprod Dev 51:167–175
43. Zhao W et al (2018) Outer dense fibers stabilize the axoneme to maintain sperm motility. J Cell Mol Med 22:1755–1768
44. Brohmann H, Pinnecke S, Hoyer-Fender S (1997) Identification and characterization of new cDNAs encoding outer dense fiber proteins of rat sperm. J Biol Chem 272:10327–10332
45. Shen Y et al (2019) Loss-of-function mutations in QRICH2 cause male infertility with multiple morphological abnormalities of the sperm flagella. Nat Commun 10:433
46. Chien YH et al (2013) Bbof1 is required to maintain cilia orientation. Development 140:3468–3477
47. Gao F et al (2006) The Wilms tumor gene, Wt1, is required for Sox9 expression and maintenance of tubular architecture in the developing testis. Proc Natl Acad Sci USA 103:11987–11992
48. Zhang Q, Ji SY, Busayavalasa K, Shao J, Yu C (2019) Meiosis I progression in spermatogenesis requires a type of testis-specific 20S core proteasome. Nat Commun 10:3387
49. Zhou J, Yang F, Leu NA, Wang PJ (2012) MNS1 is essential for spermiogenesis and motile ciliary functions in mice. Plos Genet. https://doi.org/10.1371/journal.pgen.1002516
50. Leslie JS et al (2020) MNS1 variant associated with situs inversus and male infertility. Eur J Hum Genet 28:50–55
51. Li Y et al (2021) A novel homozygous frameshift mutation in MNS1 associated with severe oligoasthenoteratozoospermia in humans. Asian J Androl 23:197–204
52. Hoyer-Fender S, Neesen J, Szpirer J, Szpirer C (2003) Genomic organisation and chromosomal assignment of ODF2 (outer dense fiber 2), encoding the main component of sperm tail outer dense fibers and a centrosomal scaffold protein. Cytogenet Genome Res 103:122–127

53. Shao X, Murthy S, Demetrick DJ, van der Hoorn FA (1998) Human outer dense fiber gene, ODF2, localizes to chromosome 9q34. Cytogenet Cell Genet 83:221–223
54. Novarino G, Akizu N, Gleeson JG (2011) Modeling human disease in humans: the ciliopathies. Cell 147:70–79
55. Reiter JF, Leroux MR (2017) Genes and molecular pathways underpinning ciliopathies. Nat Rev Mol Cell Bio 18:533–547
56. Huber D, Geisler S, Monecke S, Hoyer-Fender S (2008) Molecular dissection of ODF2/Cenexin revealed a short stretch of amino acids necessary for targeting to the centrosome and the primary cilium. Eur J Cell Biol 87:137–146
57. Sironen A, Shoemark A, Patel M, Loebinger MR, Mitchison HM (2020) Sperm defects in primary ciliary dyskinesia and related causes of male infertility. Cell Mol Life Sci CMLS 77:2029–2048
58. Leslie JS et al (2020) MNS1 variant associated with situs inversus and male infertility. Eur J Hum Genet EJHG 28:50–55
59. Li Y et al (2020) A novel homozygous frameshift mutation in MNS1 associated with severe oligoasthenoteratozoospermia in humans. Asian J Androl
60. Ta-Shma A et al (2018) Homozygous loss-of-function mutations in MNS1 cause laterality defects and likely male infertility. PLoS Genet 14:e1007602
61. Abu-Halima M et al (2021) MicroRNA-targeting in spermatogenesis: Over-expressions of microRNA-23a/b-3p and its affected targeting of the genes ODF2 and UBQLN3 in spermatozoa of patients with oligoasthenozoospermia. Andrology 9:1137–1144